Bioorganic & Medicinal Chemistry 19 (2011) 5342–5351

Contents lists available at SciVerse ScienceDirect

Bioorganic & Medicinal Chemistry

journal homepage: www.elsevier.com/locate/bmc

Biochemical characterization of a novel type-II VEGFR2 kinase inhibitor: Comparison of binding to non-phosphorylated and phosphorylated VEGFR2

Hidehisa Iwata [a], Shinichi Imamura [b], Akira Hori [b], Mark S. Hixon [c,*], Hiroyuki Kimura [a], Hiroshi Miki [a,*]

[a] Discovery Research Laboratories, Pharmaceutical Research Division, Takeda Pharmaceutical Company Ltd, 26-1, Muraoka-Higashi, 2-chome, Fujisawa, Kanagawa 251-8555, Japan
[b] Oncology Drug Discovery Unit, Pharmaceutical Research Division, Takeda Pharmaceutical Company Ltd, 26-1, Muraoka-Higashi, 2-chome, Fujisawa, Kanagawa 251-8555, Japan
[c] Takeda San Diego Inc., 10410 Science Center Drive, San Diego, CA 92121, USA

ARTICLE INFO

Article history:
Received 24 July 2011
Accepted 2 August 2011
Available online 6 August 2011

Keywords:
Vascular endothelial growth factor receptor 2
Type-II inhibitor
Slow binding mechanism
Phosphorylation

ABSTRACT

A pyrrolo[3,2-*d*]pyrimidine-based type-II vascular endothelial growth factor receptor 2 (VEGFR2) kinase inhibitor, compound **20d**, displayed time-dependent inhibition of the non-phosphorylated catalytic domain of VEGFR2. In contrast, **20d** did not show time-dependent inhibition of the phosphorylated enzyme. Dissociation of **20d** from non-phosphorylated VEGFR2 was slow and the half-life of the complex was longer than 4 h. In contrast, dissociation of **20d** from the phosphorylated enzyme was very fast (half-life <5 min). A fluorescent tracer based displacement assay and surface plasmon resonance (SPR) analysis confirmed the slow dissociation of **20d** from only non-phosphorylated VEGFR2. Thus, activity based and binding kinetic analyses both supported slow dissociation of **20d** from only non-phosphorylated VEGFR2. Additionally SPR analysis revealed that association rates were rapid and nearly identical for these two phosphorylation forms of VEGFR2. From these results, the preferential effect of **20d** on non-phosphorylated VEGFR2 is dominated by its slow dissociation from the enzyme and this characteristically long residence time may increase its potency in vivo. The present findings may assist in the design of novel type-II kinase inhibitors.

1. Introduction

The protein kinase superfamily is one of the largest and most attractive of drug targets. There are 518 known human protein kinases commonly presented as a kinome dendrogram.[1] Protein kinases play an important role in various cellular events, such as cell survival and proliferation. The receptor tyrosine kinase (RTK) family is a member of the protein kinase superfamily. Common to all RTKs is a single membrane-spanning region and a substrate specificity of tyrosine as the phosphate acceptor on their protein substrates. The activity of RTKs is tightly repressed until the receptor is stimulated by its ligand through a cis inhibition/trans activation mechanism.[2] The equilibrium between inactive and active conformations of the non-phosphorylated RTK in solution shifts toward the active conformation upon ligand binding.[3] The activation state of the enzyme may be defined with respect to the conformation of an activation loop. In the inactive state, the Asp-Phe-Gly sequence (DFG motif) at the beginning of this activation loop of the RTK flips out interfering with substrate access to the active site.[4] This inactive conformation is called a DFG-out conformation. After stimulation by its ligand, each RTK dimerizes as homodimers or heterodimers. Dimerization triggers the autophosphorylation of tyrosine residues including those located within the activation loop so-called because their phosphorylation is required for enzyme activation. Autophosphorylation of the activation loop residues shifts the equilibrium toward the active conformation and drives the DFG motif to its in conformation, facilitating substrate access to the active site. This active conformation is called the DFG-in conformation.

Among various protein kinase inhibitors, some are categorized by their mode of binding with the target kinase, such as whether the inhibitor shows a preference for binding to the active or inactive conformation of the enzyme. Type-I inhibitors bind within the ATP-binding site and form hydrogen bonds with the kinase hinge region.[5] These inhibitors are thought to bind with equal avidity to both the active and inactive forms of the target kinase. Thus type-I inhibitors inhibit the target enzyme independent of the phosphorylation/activation state of the target tyrosine kinases.

Abbreviations: IC_{50}, 50% inhibitory concentration; ATP, adenosine 5′-triphosphate; DMSO, dimethyl sulfoxide; DTT, DL-dithiothreitol; EDTA, ethylenediamine-*N*,*N*,*N*′,*N*′-tetraacetic acid; $MgCl_2$, magnesium chloride; $MnCl_2$, manganese chloride; Tris, tris(hydroxymethyl)aminomethane; Tween-20, polyoxyethylene(20)sorbitan monolaurate; VEGFR, vascular endothelial growth factor receptor; PDGFR, platelet-derived growth factor receptor.

* Corresponding authors. Addresses: 10410 Science Center Drive, San Diego, CA 92121, USA. Tel.: +1 858 731 3578; fax: +1 858 550 0526 (M.S.H.); 26-1, Muraoka-Higashi, 2-chome, Fujisawa, Kanagawa 251-8555, Japan. Tel.: +81 466 32 2747; fax: +81 466 29 4484 (H.M.).

E-mail addresses: mark.hixon@takedasd.com (M.S. Hixon), Miki_Hiroshi@takeda.co.jp (H. Miki).

0968-0896/$ - see front matter © 2011 Elsevier Ltd. All rights reserved.
doi:10.1016/j.bmc.2011.08.002

On the other hand, type-II inhibitors promote adoption of the inactive form of the target kinase. These inhibitors bind within the canonical ATP-binding site of the kinase domain and cause the enzyme to adopt an inactive-like conformation, such as a DFG-out conformation of the activation loop or a C-helix-out conformation. Type-II inhibitors also interact with a deeper region of the target kinase called the back pocket or deep pocket site. The first of these inhibitors to become a therapeutic agent was Imatinib (Gleevec®, Novartis, Switzerland) that binds with Abelson tyrosine kinase (Abl) causing it to adopt a DFG-out conformation.[6,7] Imatinib was the first type-II inhibitor approved for chronic myeloid leukemia. One of the advantages of the type-II inhibitors over common ATP-binding site inhibitors is slower dissociation.[8,9] With respect to selectivity, type-II inhibitors might offer an advantage over traditional type-I inhibitors since type-II inhibitors bind to an inactive form that is more likely to be a distinctive characteristic of the target kinase.[10] Of course, those protein kinases sharing similar inactive structures, type-II inhibitors are not anticipated to show higher selectivity than type-I inhibitors.[11] The potential advantage of type-II over type-I inhibitors with respect to selectivity has yet to be resolved. However, utilizing an inactive-like conformation of the target kinase is a very reasonable alternative approach to the traditional kinase inhibitor optimization that drives on an active conformation in the development of kinase inhibitors. Since opportunities may exist to overcome issues of kinase selectivity or intellectual property, it is important to evaluate how candidate compounds inhibit the inactive form of the enzyme.[10,12] Slow binding inhibition is conventionally defined by one of two common mechanisms that are described in Schemes 1 and 2. Scheme 1 represents a one-step binding mechanism with a slow association rate constant (k_1) and an even slower dissociation rate constant (k_2), leading to the slow onset of inhibition. Characteristic of this mechanism is a k_{on} that is non-saturable with respect to inhibitor concentration. Inhibition of angiotensin-converting enzyme by captopril or enalapril is consistent with this one-step binding inhibition mechanism.[13] In contrast, the two-step binding mechanism illustrated in Scheme 2 involves two steps to reach the final equilibrium enzyme–inhibitor complex. The initial enzyme–inhibitor (EI) complex forms rapidly and then slowly proceeds to a more stable enzyme–inhibitor complex (EI*). In this scheme, observed slow binding is governed by a slowly reversible isomerization rate constant (k_4). The inhibition of HIV-1 integrase by L-870,810 is an example of two-step binding inhibition.[14]

Although some studies of the binding mode of type-II kinase inhibitors have been reported, the mechanism of their slow binding inhibition has not yet been clarified as one- or two-step slow binding inhibition and few biochemical analyses have been reported. We have reported that **20d** (Fig. 1A) is a vascular endothelial growth factor receptor/platelet-derived growth factor receptor (VEGFR/PDGFR) inhibitor with slow dissociation from VEGFR2.[15] Previously,[16] we reported that TAK-593 and Sorafenib (Nexavar®, Bayer), are also slow binding and most consistent with a two step mechanism against the cytoplasmic domain of unactivated VEFGR2. In this study, we have evaluated the detailed biochemical characteristics of **20d** assessing its interactions with the phosphorylated and non-phosphorylated forms of VEGFR2 protein. Our results demonstrate that **20d** preferentially inhibits non-phosphorylated VEGFR2 with a residence time on the order of hours and that its mechanism of action for non-phosphorylated VEGFR2 involves two-step binding inhibition. Because of these characteristics, **20d** may show prolonged inhibitory activity against VEGFR2 both in vitro and in vivo.

$$E + I \underset{k_2}{\overset{k_1}{\rightleftharpoons}} EI$$

Scheme 1. One-step slow binding mechanism.

$$E + I \underset{k_2}{\overset{k_1}{\rightleftharpoons}} EI \underset{k_4}{\overset{k_3}{\rightleftharpoons}} E^*I$$

Scheme 2. Two-step slow binding mechanism.

2. Results

2.1. Phosphorylation state of VEGFR2

To confirm the phosphorylation state of VEGFR2 with or without an autophosphorylation step, Western blot analysis and LC/MS were performed (Fig. 2, Supplementary Fig. S2). From the results of Western blotting, VEGFR2 protein was phosphorylated at residues Tyr1054 and Tyr1059 of its activation loop in the autophosphorylation experiment. These two residues are reported to be the residues responsible for enzyme activation.[17] On the other hand, the purified protein without autophosphorylation did not display corresponding bands in immunoblotting experiments using anti-phospho VEGFR2 antibody as the primary antibody. LC/MS analysis revealed a single main peak of non-phosphorylated VEGFR2 and two main peaks of phosphorylated VEGFR2. There was a difference of 480 and 558 Da between the non-phosphorylated VEGFR2 peak and each peak of phosphorylated VEGFR2. These differences indicate that phosphorylated VEGFR2 has six to seven more phoshphorylated amino acids than the non-phosphorylated enzyme.

2.2. Pre-incubation time-dependent inhibition by 20d

Compound **20d** is a selective VEGFR/PDGFR inhibitor, as previously reported by Oguro et al.[15] and its inhibitory activity toward

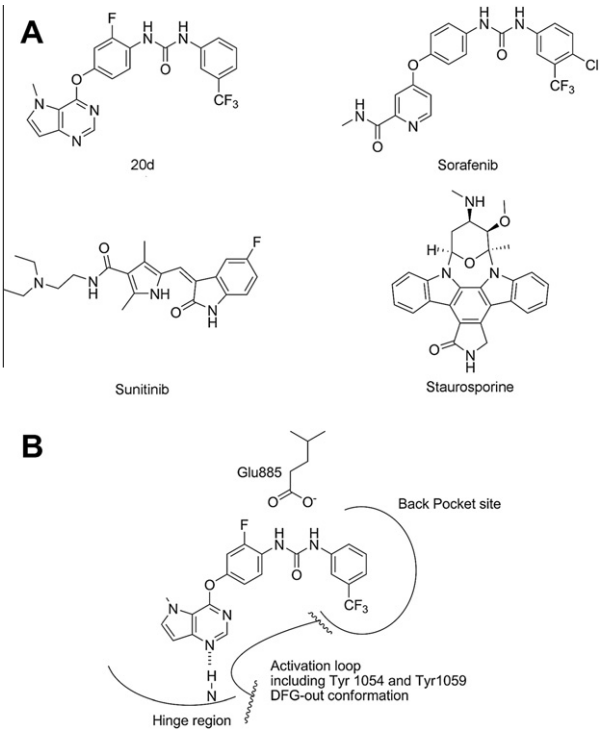

Figure 1. (A) Chemical structures of **20d**, Staurosporine, Sunitinib (Sutent), and Sorafenib (Nexavar). (B) VEGFR2 ATP binding pocket illustrating the relevant binding interactions and activation loop. Crystal structure of VEGFR2 and **20d** complex was reported previously.[15]

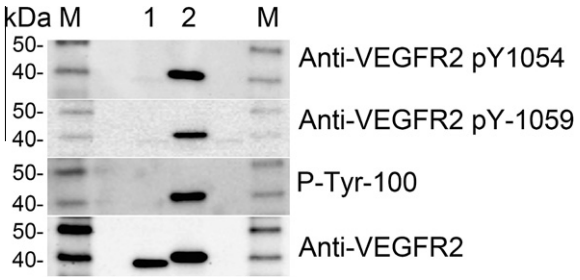

Figure 2. Western blot analysis of phosphorylation of tyrosine residues on VEGFR2. Non-phosphorylated VEGFR2 (lane 1) and phosphorylated VEGFR2 (lane 2) were subjected to Western blot analysis using anti-phospho-VEGFR2 tyrosine 1054 antibody, anti-phospho-VEGFR2 tyrosine 1059 antibody, P-Tyr-100 antibody, and anti-VEGFR2 antibody. M; Molecular markers.

cellular proliferation of human umbilical vein endothelial cells is 4.4 nM. Binding interactions with VEGFR2 span from the hinge region to a back pocket site of the enzyme, thus **20d** is categorized as a type-II kinase inhibitor (Fig. 1B). As shown in Figure 3, **20d** inhibition is ATP-competitive for both the phosphorylated and the non-phosphorylated catalytic domain of VEGFR2. Characterization of a type-II kinase inhibitor requires an examination of inhibitory activity against the target kinases in different states of phosphorylation. By examining both the non-phosphorylated catalytic domain and the autophosphorylated catalytic domain of VEGFR2, we compared the inhibitory activity of **20d** and its mechanism of action.

Compound **20d** displayed no significant time-dependence in its inhibition of phosphorylated VEGFR2 (Fig. 4E and Table 1). The IC_{50} was 46 nM (K_i = 23 nM by use of the Cheng Prusoff equation) without pre-incubation and it displayed a rapid equilibrium binding mechanism for phosphorylated VEGFR2. In contrast, pre-incubation experiments with non-phosphorylated VEGFR2 produced IC_{50} values of **20d** that decreased as the pre-incubation time increased. For example, **20d** inhibited non-phosphorylated VEGFR2 with an IC_{50} of 4.7 nM in the absence of pre-incubation yet after 120 min pre-incubation, the IC_{50} decreased to 33 pM. Thus, at final equilibrium, **20d** displayed about 140-fold greater potency over that of its initial binding complex (Fig. 4A and Table 1).

A detailed kinetic investigation of the onset of the tight-binding enzyme–inhibitor complex (EI*) formation proved challenging. The unactivated (non-phoshorylated) form of VEGFR2 has less than 5% of the catalytic activity (k_{cat}/K_m) of activated VEGFR2. In addition, auto-activation is a competing side reaction when examining enzyme catalysis. The enzyme activity of a few percent of activated VEGFR2 will eclipse the activity of the un-activated enzyme. Auto-activation of VEGFR2 goes as the square of its concentration hence working at low enzyme concentration minimizes this undesired side reaction. Additionally, following the enzyme activity over a narrow time window (10 min) reduces the contribution of product from any activated enzyme present by limiting the formation of activated enzyme. Lastly, working with lower competitive substrate (ATP) also mitigates the amount of auto-activation. Under such circumstances, we were compelled to use a pre-incubation approach followed by a minimal dilution endpoint assay with high sensitivity. In these experiments, the onset of the tight enzyme inhibitor complex occurs in pre-incubation phase as well as in the enzyme activity phase. Equations describing progress curves that account for the onset of tight binding through both phases of the assay were required. Since inhibitor dissociation was very slow relative to the practical pre-incubation times that can be examined and that the final enzyme–inhibitor complex is

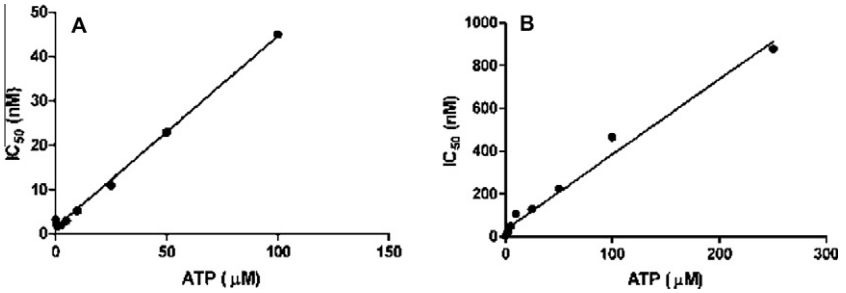

Figure 3. Compound **20d** shows ATP-competitive inhibition of VEGFR2. IC_{50} values of **20d** versus the ATP concentration for non-phosphorylated VEGFR2 (A) and phosphorylated VEGFR2 (B). Experiments to determine the IC_{50} values were performed with the AlphaScreen system in quadruplicate.

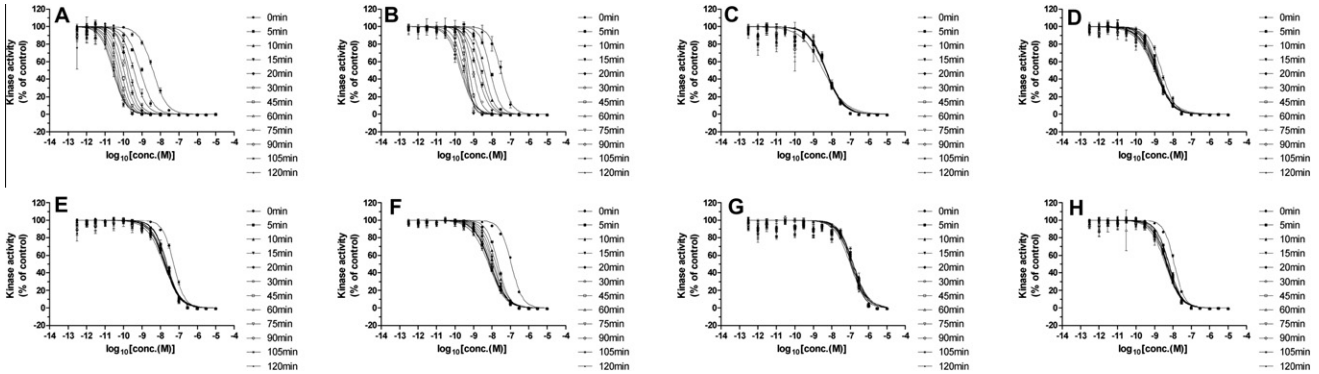

Figure 4. Effect of pre-incubation time on the inhibitory activity of **20d** (A, E), Sorafenib (B, F), Sunitinib (C, G), and Staurosporine (D, H). Concentration dependent inhibition curves for each compound with various enzyme and inhibitor pre-incubation times for non-phosphorylated VEGFR2 (A, B, C, and D) and phosphorylated VEGFR2 (E, F, G, and H). All experiments were performed with the AlphaScreen system. Data represent the mean ± SD (n = 4). These are representative results from three independent experiments.

Table 1
Inhibition of VEGFR2 kinase activity with and without pre-incubation

	Non-phosphorylated VEGFR2 IC_{50}[a] (nM)		Phosphorylated VEGFR2 IC_{50}[a] (nM)	
	0 min	120 min	0 min	120 min
20d	4.7 (1.3)	0.033 (0.017)	46 (7.3)	14 (3.0)
Sorafenib	23 (5.9)	0.16 (0.046)	100 (18)	6.2 (1.1)
Sunitinib	5.7 (2.5)	5.5 (1.3)	147 (51)	98 (11)
Staurosporine	3.4 (1.2)	1.2 (0.41)	11(1.4)	3.8 (0.51)

[a] Estimated IC_{50} values (SD in parentheses) derived from three independent experiments.

very tight, the progress curves take on the appearance of irreversible inhibition. Such conditions can make the dissociation rate constant parameter ill-defined therefore equations for the global fitting of the progress curves were examined that included an inhibitor dissociation rate constant and with the dissociation rate constant set to zero. Eqs. (1a)–(1d) (Section 5) describe single step binding with no dissociation 1a, single step binding that includes dissociation 1b, two step no dissociation 1c and two step with dissociation 1d under our assay conditions. Full derivations are found in Supplementary data. Pre-incubating a gradient of **20d** concentrations over a range of times and then fitting the progress curves globally confirmed that the dissociation rate constant could not be determined reliably. The system was best described by Eq. 1c, that is, two step binding with $k_4 = 0$. From the above analysis, a K_i of 4.6 ± 0.2 nM was obtained which is in good agreement with the IC_{50} with no pre-incubation (activity assay time = 10 min) (Table 1). The transition rate constant (k_3) from loose binding to tight binding was $9.0 \times 10^{-3} \pm 4 \times 10^{-4}$ s^{-1} affording a half life for the transition of approximately 1.3 min at saturating **20d**.

Staurosporine, a non-selective kinase inhibitor, and two clinically available multi-kinase inhibitors, Sorafenib and Sunitinib (Fig. 1) were also examined for time-dependent binding. Like **20d**, Sorafenib inhibited non-phosphorylated VEGFR2 in a time-dependent manner (Fig. 4B and Table 1). Global analysis of the inhibition onset progress curves was also best described by Eq. 1c with k_4 constrained to zero. The initial binding complex has a K_i of 22 ± 2 nM and a transition rate constant (k_3) from loose binding to tight binding of $7.1 \times 10^{-3} \pm 6 \times 10^{-4}$ s^{-1} affording a half life for the transition of approximately 1.6 min at saturating Sorafenib.

Interestingly, there was also modest time dependency of the inhibition of phosphorylated VEGFR2 by Sorafenib. We could not determine the kinetic parameters for inhibition of phosphorylated VEGFR2 by Sorafenib since its binding was too rapid to analyze by these methods. In contrast, Staurosporine and Sunitinib inhibited non-phosphorylated VEGFR2 with a rapid equilibrium binding mechanism (Fig. 4C and D and Table 1). Surprisingly, Sunitinib was 20-fold selective for non-phosphorylated VEGFR2 even though it is classified as a type-I kinase inhibitor.

2.3. Dissociation rate constant obtained with rapid large dilution

To determine the dissociation rate constant (k_{off}), we performed rapid large dilution assays[18] with the non-phosphorylated and phosphorylated enzymes. As predicted from the analysis of pre-incubation time dependence, **20d** displayed very slow dissociation from the non-phosphorylated catalytic domain of VEGFR2 with a k_{off} was 4.6×10^{-5} s^{-1} translating into a half life of 4.3 h (Fig. 6A and Table 3). In contrast, **20d** displayed rapid dissociation from the phosphorylated catalytic domain of VEGFR2 and its k_{off} was greater than the detection limit of the dissociation assay. Therefore, its k_{off} is $>2.3 \times 10^{-3}$ s^{-1} and the dissociation half-life is less than 5 min (Fig. 6B and Table 3). Like **20d**, Sorafenib displayed slow dissociation from non-phosphorylated VEGFR2 having a k_{off} value of 6.7×10^{-6} s^{-1} (Fig. 6A and Table 3). Moreover, as observed in the study of pre-incubation time dependence, Sorafenib dissociated more slowly from phosphorylated VEGFR2 than did **20d** (Fig. 6B). With the type-I inhibitors (Sunitinib and Staurosporine), there was rapid recovery of the activity of both non-phosphorylated and phosphorylated VEGFR2 (k_{off} values $>2.3 \times 10^{-3}$ s^{-1}), affording dissociation half-lives of less than 5 min (Fig. 6A and B and Table 3). From these results, the type-I inhibitors dissociated rapidly regardless of the phosphorylation state of their target kinase.

As an orthogonal approach, a fluorescent tracer displacement assay was employed to obtain k_4. Enzyme was pre-incubated with inhibitor attaining equilibrium and then diluted 100-fold. Displacement of inhibitor by the tracer resulted in an increase in observed fluorescence which could be followed continuously. (Fig. 6C) Since this methodology does not require enzymatic activity, there is no concern over enzyme autophosphorylation from the presence of ATP during the progress of the assay. From the tracer-based displacement assays, **20d** and Sorafenib slowly dissociated from non-phosphorylated VEGFR2 possessing k_{off} values of 8.7×10^{-5} and 4.0×10^{-5} s^{-1}, respectively (Table 3). On the other hand, both of type-II kinase inhibitors rapidly dissociated from phosphorylated VEGFR2 (Fig. 6D) affording k_{off} values for **20d** and Sorafenib of $>2.3 \times 10^{-3}$ and 7.3×10^{-4} s^{-1}, respectively (Table 3). Results were consistent with the activity-based k_{off} determinations above with the exception of non-phosphorylated VEGFR2 Sarfenib k_{off} which was 6-fold faster in this assay.

By use Eq. 2 and the obtained values for K_i, k_3, obtained from inhibition onset experiments and k_4 obtained from k_{off} experiments, we calculated the final equilibrium dissociation constants K_i^* for **20d** and Sorafenib and have presented these values in Table 2. Two solutions for K_i^* are obtained based on which experimental determination of k_4 is selected. The average value from the two solutions of K_i^* for **20d** is 29 pM and is very close to the Cheng Prusoff equation calculated K_i of 18 pM obtained after 120 min pre-incubation. There was greater variation in the two

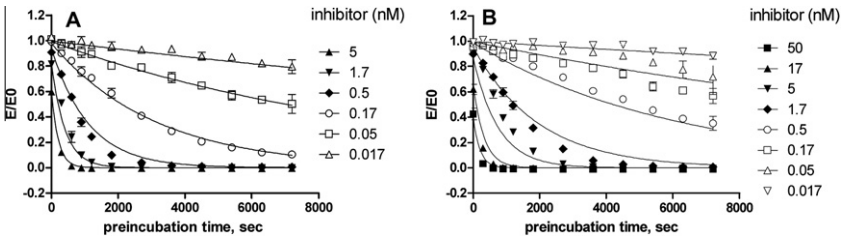

Figure 5. Replots of data from the pre-incubation experiments displayed in Figure 4. Activity of non-phosphorylated VEGFR2 as a function of pre-incubation time was globally fitted to Eq. 1c to obtain kinetic parameters for **20d** (A) and Sorafenib (B) Data represent the mean ± SD ($n = 4$). These plots show representative data from three independent experiments.

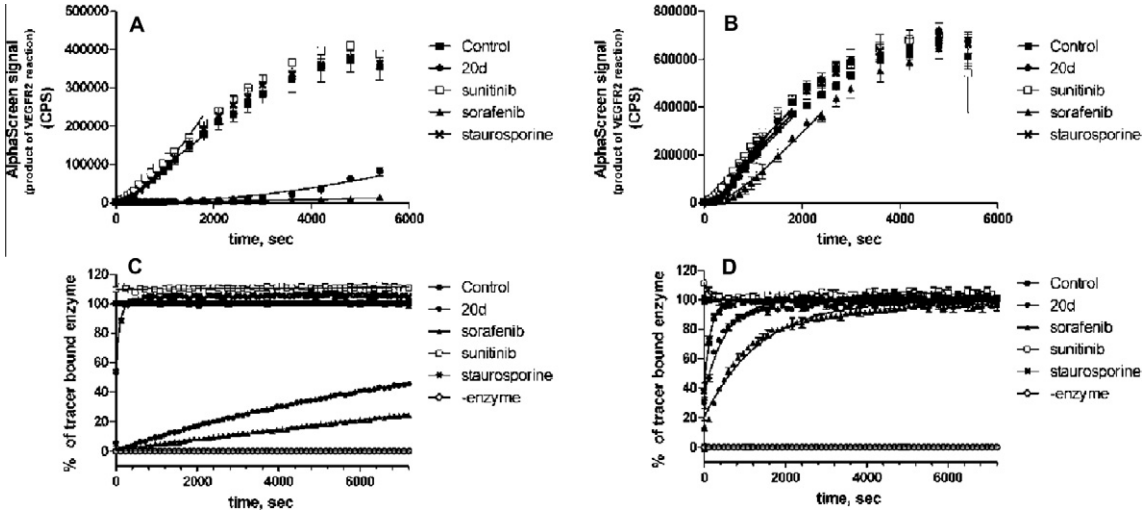

Figure 6. Recovery of enzyme activity (A and B) and tracer binding activity (C and D) after 100-fold dilution for estimation of dissociation rate constants. (A) Results of the activity based the 100-fold dilution assay with non-phosphorylated VEGFR2 and **20d** (●), Staurosporine (×), Sorafenib (▲), Sunitinib (□), or no inhibitor as a control (■). (B) Results of activity based the 100-fold dilution assay with phosphorylated VEGFR2 and **20d** (●), Staurosporine (×), Sorafenib (▲), Sunitinib (□), or no inhibitor as a control (■). (C) Results of the fluorescent tracer based 100-fold dilution assay with non-phosphorylated VEGFR2 and **20d** (●), Staurosporine (×), Sorafenib (▲), Sunitinib (□), or without any inhibitor as a control (■) and without inhibitor or enzyme (○). (D) Results of the fluorescent tracer based 100-fold dilution assay with phosphorylated VEGFR2 and **20d** (●), Staurosporine (×), Sorafenib (▲), Sunitinib (□), or without any inhibitor as a control (■) and without inhibitor or enzyme (○). Representative data from three independent experiments are shown. Results represent the mean ± SD (n = 3).

Table 2
Kinetic constants from pre-incubation experiments with non-phosphorylated VEGFR2

	K_i[a] (nM)	K_i*[b] (nM)	K_i*[c] (nM)	k_3[a] (s^{-1})
20d	4.6 (0.2)	0.024	0.044	9.0×10^{-3} (4.0×10^{-4})
Sorafenib	22 (1.9)	0.021	0.120	7.1×10^{-3} (6.3×10^{-4})
Sunitinib	2.9[d]	N.D.	N.D.	N.D.
Staurosporine	1.7[d]	N.D.	N.D.	N.D.

[a] Global fit to inhibition onset progress curves to obtain K_i and k_3 values (SD in parentheses).
[b] Values calculated by Eq. 2 using K_i, k_3, and k_4 from activity based analysis.
[c] Values calculated by Eq. 2 using K_i, k_3, with k_4 from ligand displacement based analysis.
[d] Sunitinib and Staurosporine are not time dependent inhibitors, K_i values calculated from IC_{50} values with no pre-incubation are shown.

calculations of K_i^* for Sorafenib but the average value of 70 pM matches Cheng Prusoff equation calculated K_i of 80 pM.

The slow dissociative character of **20d** and Sorafenib from only non-phosphorylated VEGFR2 are confirmed two assay methodologies. The k_{off} value of **20d** for dissociation from non-phosphorylated VEGFR2 was at least 50-fold smaller than the k_{off} for phosphorylated VEGFR2, and the difference was much larger for Sorafenib (about 200-fold). These results suggest that both of the type-II kinase inhibitors investigated in this study were recognized by non-phosphorylated and phosphorylated VEGFR2 but their dissociation velocity are highly affected by the state of phosphorylation of the bound enzyme.

2.4. Surface plasmon resonance (SPR) analysis

In the activity based and fluorescent tracer displacement experiments, **20d** only displayed time-dependent inhibition and slow dissociation in the case of non-phosphorylated VEGFR2. In order to evaluate these characteristics of **20d** through binding kinetics, we performed SPR analysis using a Biacore biosensor with non-phosphorylated and phosphorylated VEGFR2. The sensorgrams are presented in Figure 7. Unfortunately, the sensorgram traces for **20d** against non-phosphorylated enzyme defied fitting to reasonable models. As such, they are best viewed qualitatively. SPR analysis captures transitions that are much faster than what is observable by the methods described above. From the sensorgrams it is clear that onset of the EI complex was not rapid equilibrium (on the SPR time scale) for either non-phosphorylated enzyme or the phosphorylated enzyme. As observed in the pre-incubation and dilution experiments, **20d** dissociation from the non-phosphorylated enzyme was considerably slower (indeterminately slow by Biacore) than dissociation from the phosphorylated enzyme. Qualitatively, the two step slow binding mechanism reveals itself in the

Table 3
Kinetic constants for non-phosphorylated and phosphorylated VEGFR2from enzyme–inhibitor complex dilution assays

	Method	Non-phosphorylated VEGFR2		Phosphorylated VEGFR2	
		k_{off}[a] (s^{-1})	$t_{1/2}$[b] (min)	k_{off}[a] (s^{-1})	$t_{1/2}$[b] (min)
20d	Activity based	4.6×10^{-5} (8.9×10^{-6})	260 (55)	$>2.3\times10^{-3}$[c]	<5
	Ligand displacement	8.7×10^{-5} (6.5×10^{-6})	130 (10)	$>2.3\times10^{-3}$[c]	<5
Sorafenib	Activity based	6.7×10^{-6} (1.7×10^{-6})	1800 (510)	1.5×10^{-3} (4.2×10^{-4})	8 (3)
	Ligand displacement	4.0×10^{-5} (2.9×10^{-6})	290 (20)	7.3×10^{-4} (2.8×10^{-4})	18 (9)
Sunitinib	Activity based	$>2.3\times10^{-3}$[c]	<5	$>2.3\times10^{-3}$[c]	<5
	Ligand displacement	$>2.3\times10^{-3}$[c]	<5	$>2.3\times10^{-3}$[c]	<5
Staurosporine	Activity based	$>2.3\times10^{-3}$[c]	<5	$>2.3\times10^{-3}$[c]	<5
	Ligand displacement	$>2.3\times10^{-3}$[c]	<5	$>2.3\times10^{-3}$[c]	<5

[a] Estimated k_{off} values (SD in parentheses).
[b] Values calculated with Eq. 3 using k_{off} values (SD in parentheses).
[c] Values calculated with Eq. 3 using $t_{1/2}$ < 5 min. Results shown were derived from three independent experiments.

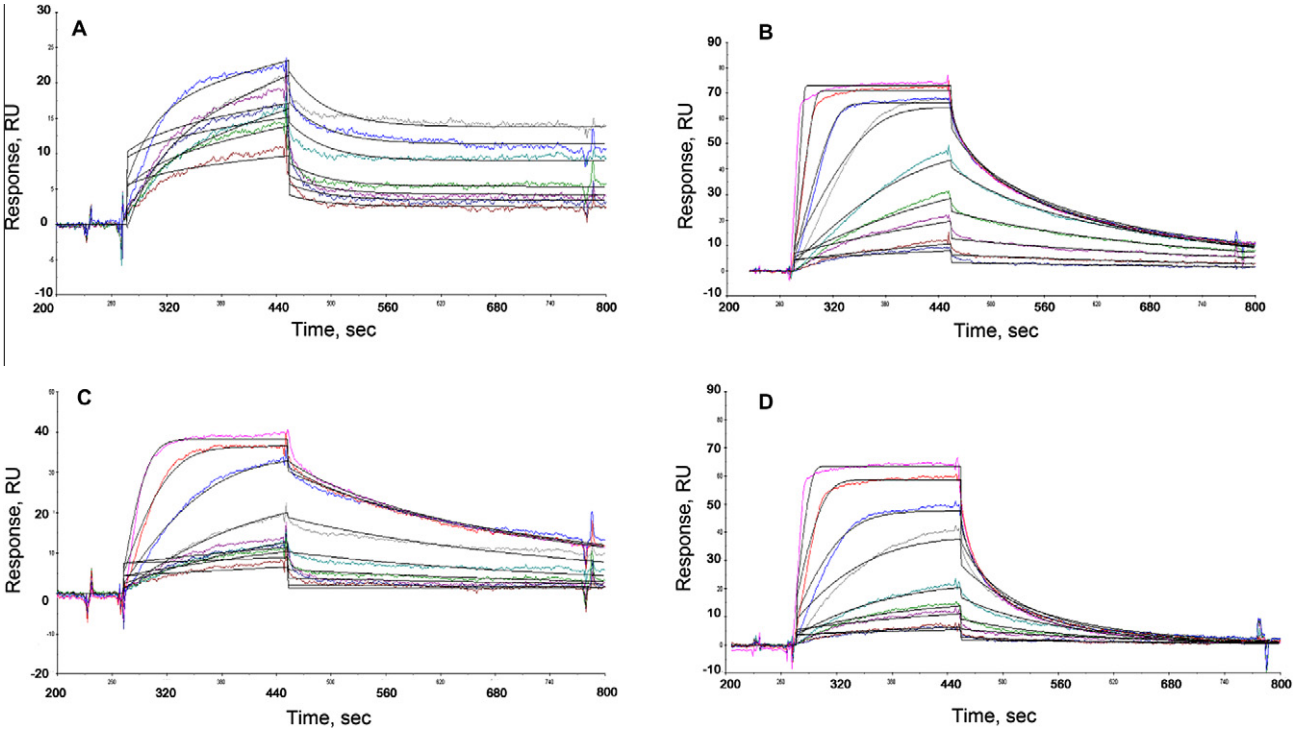

Figure 7. Results of SPR binding experiments with non-phosphorylated VEGFR2 (A, B) and phosphorylated VEGFR2 (C, D). **20d** was injected at 2-fold serial dilutions from 1.9 to 125 nM for non-phosphorylated VEGFR2 (A) and 2-fold serial dilutions from 1.9 to 500 nM for phosphorylated VEGFR2 (C). Sunitinib was injected at 2-fold serial dilutions from 1.9 to 500 nM for both non-phosphorylated VEGFR2 (B) and phosphorylated VEGFR2 (D). (A) Each sensorgram was globally fitted to a two-state reaction (conformation change) model except for R_{max} values that were obtained by local fitting to the same binding model. (B), (C), and (D) Each sensorgram was fitted to a 1:1 binding with mass transfer model, except for R_{max} value that were obtained by local fitting to the same binding model. These results are representative data from three independent experiments.

biphasic nature of inhibitor dissociation from the enzyme-bound complex. The loose (rapidly reversible) complex quickly dissociates while the EI* tight complex dissociates very slowly on the Biacore time scale (Fig. 7). Curiously, Sorafenib, the other slow binding inhibitor, sensorgram traces also defied fitting to reasonable models (Fig. S3). In contrast, the sensorgrams for dissociation of Sunitinib from non-phosphorylated VEGFR2 fit well to a 1:1 single step binding model (Fig. 7B). Moreover, the sensorgram of **20d** for phosphorylated VEGFR2 fit a 1:1 single step binding model well (Fig. 7C). K_a and K_d values of **20d** for phosphorylated VEGFR2 were determined as $1.6 \times 10^5 M^{-1} s^{-1}$ and $3.1 \times 10^{-3} s^{-1}$, respectively. With these parameters, K_D was calculated as 19 nM. The K_D is good agreement with K_i of 23 nM from enzymatic activity based analysis. Additionally, **20d** preferentially interacts with non-phosphorylated VEGFR2, as observed in the activity based experiments, and this preference seems to be based on the difference of dissociation rate constants for non-phosphorylated and phosphorylated VEGFR2 (Fig. 7A and C). Interestingly, Sunitinib also demonstrated a preference for non-phosphorylated VEGFR2 as observed in activity based experiments. The K_D value for non-phosphorylated VEGFR2 obtained with steady state affinity analysis was about 5-fold smaller than K_D value for the phosphorylated enzyme.

2.5. Cellular autophosphorylation assay

We assessed the inhibitory activity of **20d** in a cellular autophosphorylation assay using 293/KDR cells that stably over expressed VEGFR2, but whose proliferation and survival were VEGF independent. Since autophosphorylation of tyrosine 1175 is considered a requirement for VEGF mediated survival and proliferation,[20] we used phosphorylation of this residue to index of cellular VEGFR2 kinase activity. Phosphorylation was detected by

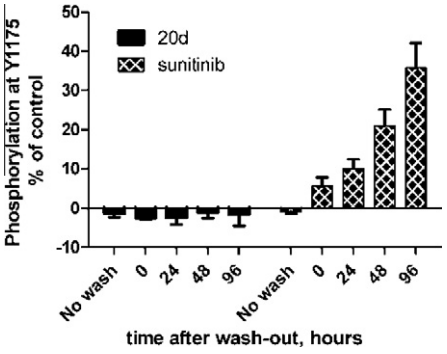

Figure 8. Recovery of autophosphorylation of tyrosine residues on VEGFR2 after washout of inhibitor. Serum starved KDR/293 cells were incubated with **20d** or Sunitinib at 100 nM for 1 h, and then washed with inhibitor-free medium. Next, the cells were stimulated with 50 ng/ml of VEGF for 10 min at the indicated times after washout, followed by lysis with cell lysis buffer. Total cell lysates were subjected to ELISA with phospho tyrosine 1175 antibody. Values were normalized from 0% (the well containing no inhibitor and without VEGF stimulation) to 100% (the well containing no inhibitor and with VEGF stimulation). Data are shown as the mean and SD ($n = 3$).

an enzyme-linked immunosorbent assay (ELISA). As shown in (Fig. 8), **20d** and Sunitinib both completely inhibited VEGF-induced autophosphorylation of tyrosine 1175 on VEGFR2 at 100 nM without an inhibitor washout step. Even at 96 h post inhibitor washout, compound **20d** completely inhibited VEGF-stimulated phosphorylation of VEGFR2. In marked contrast washout experiments with Sunitinib displayed an increasing VEGFR2 phosphorylation over time post washout. Clearly **20d** displays prolonged inhibitory activity with a long residence time on VEGFR2 in a cellular assay—typical characteristics of a type-II kinase inhibitor.

3. Discussion

In this study, we used VEGFR2 to characterize the inhibitory activity of type-I and type-II kinase inhibitors and to investigate the reason for the differing inhibitory activity of type-II kinase inhibitors for non-phosphorylated and phosphorylated enzymes. First, we determined the phosphorylation state of the catalytic domain of VEGFR2 with or without autophosphorylation. The catalytic domain of VEGFR2 that we targeted in this study has 10 tyrosine residues. Among these 10 residues, it has been reported that at least 3 residues can be phosphorylated[21] and it seems that tyrosine 1008 might be phosphorylated according to a study of the mouse ortholog enzyme.[22] From our LC/MS data, there could be as many as 6 or 7 phosphorylated residues after autophosphorylation over the surface of the enzyme (Fig. S2). The in vivo presence or relevance hyperphosphorylation is unknown. However, our immunoblotting analysis indicated that relevant tyrosine residues on the activation loop of the catalytic domain of VEGFR2 underwent autophosphorylation and there was an obvious difference of phosphorylation between non-phosphorylated and phosphorylated VEGFR2 (Fig. 2). Thus, we chose to use these two proteins to characterize type-I and type-II kinase inhibitors.

We are compelled to evaluate the unactivated enzyme activity over a short time period (10 min or less) since longer reaction times will cause an unintended autoactivation through autophosphorylation. The competition of autophoshophorylation with phosphorylation of the intended peptide substrate prevented us from employing a more conventional technique to characterize k_{on} such as progress curve analysis. To address these necessities of assay sensitivity and avoidance of autoactivation, we performed enzyme assays in AlphaScreen® platform. This approach gave the desired high sensitivity when performed with $MnCl_2$ containing buffer in addition to $MgCl_2$ since the catalytic activity of VEGFR2 kinase increased.[23] In addition, we have derived equations that describe the predicted progress curves for the onset of inhibition for 2-phase assay system containing a pre-incubation phase and an assay phase where inhibition onset still continues but at a reduced rate.

Characterization of the kinase inhibitors within this study was by use of enzymatic activity and biophysical analyses. As described previously,[16] during the course of compound optimization, we perform assays with the un-phosphorylated/inactive enzyme assessing the inhibitory activity of compounds toward this enzyme form. Moreover, as observed in this study, since most type-II inhibitors preferentially inhibit non-phosphorylated enzyme, screening solely against the activated form of the enzyme may underestimate a compound's potential in vivo affinity.

As described above, one of the characteristics of type-II inhibitors is interaction with the back pocket site of the target enzyme. This binding mode not only applies to non-phosphorylated VEGFR2 but also to phosphorylated VEGFR2 according to a X-ray crystallographic study performed by using a urea based type-II kinase inhibitor and the auto-phosphorylated catalytic domain of VEGFR2.[24] Thus crystallographic data support the hypothesis that phosphorylated VEGFR2 can be induced to adopt DFG-out conformation in the presence of an inhibitor. Also, binding with the DFG-out conformation of the kinase is not sufficient to cause slow dissociation of an inhibitor since there have been some reports of type-II kinase inhibitors that do not display slow dissociation.[25] Therefore, there is no clear conclusion that the slow dissociation is coupled to the movement of the activation loop from DFG-in form to DFG-out forms of protein conformation.

In this study, we report that **20d** is a two-step slow binding inhibitor against non-phosphorylated VEGFR2, but not for phosphorylated VEGFR2, by activity based experiments (Figs. 4A, E and 5). By use of an activity based dilution assay and by use of a fluorescent tracer displacement based dilution assay, we observe that **20d** very slowly dissociated from non-phosphorylated VEGFR2 (Fig. 6A and C) yet its dissociation from phosphorylated VEGFR2 was rapid (Fig. 6B and D). These results were also observed with the other type-II inhibitor Sorafenib (Figs. 4B, F and 6). From these analysis, we obtained K_i^* of each type-II inhibitor. Except for K_i^* of Sorafenib by use of k_4 from activity based analysis, obtained K_i^* values were in good agreement with IC_{50} with 120 min pre-incubation. The discrepancy of k_4 of Sorafenib from each experiment is thought to be due to limitations of each method, such as minimal dissociation or reactivation of the enzyme.

These observations were confirmed through binding SPR-based biophysical experiments (Fig. 7). However, we could not determine whether or not the slow binding isomerization step represents a conformational change from DFG-in to DFG-out, so further studies of VEGFR2 protein or of protein–inhibitor complex conformations will be required for a more complete understanding.

Studies on the interaction of type-II kinase inhibitors with p38α MAP kinase were previously performed by use of NMR[26,27] and it was concluded that type-II inhibitors only bind p38α in the DFG-out conformation. In contrast, Frembgen–Kesner and Elcock recently reported that type-II kinase inhibitors not only bind to the DFG-out conformation of p38α MAP kinase but also the DFG-in conformation, and they suggested the existence of pseudo-DFG-in and pseudo-DFG-out conformations in addition to the generally accepted DFG-in and DFG-out conformations through analysis with molecular dynamics simulation.[28] According to the latter result, we suggest that type-II kinase inhibitors bind to the DFG-in conformation first and this may then cause a conformational change of the target enzyme.[29]

As discussed above, it is widely believed that phosphorylated VEGFR2 adopts mainly a DFG-in conformation in solution. This study strongly supports the hypothesis that type-II kinase inhibitors bind to the DFG-in conformation first since **20d** has similar binding rates for non-phosphorylated and phosphorylated VEGFR2. Upon obtaining binding equilibrium with **20d**, both the non-phosphorylated VEGFR2 and phosphorylated protein adopt DFG-out conformation and thereby only the non-phosphorylated VEGFR2 adopts a more stable and inactive conformation.

A similar phenomenon was observed in the study of PYK2 and BIRB-796, a p38α MAP kinase inhibitor.[19] BIRB-796 is known to slowly dissociate from p38α[9] but it did not show slow dissociative character with PYK2. In this study, we demonstrated that type-II inhibitors may associate at similar rates with both non-phosphorylated VEGFR2 and phosphorylated VEGFR2 and that the type-II inhibitors display slow dissociative character from the non-phosphorylated enzyme.

Although p38α MAP kinase requires phosphorylation of its threonine residues by MKK6 to display enzymatic activity, the intracellular domain or catalytic domain of RTKs like VEGFR2 has kinase activity even without phosphorylation of the activation loop. Thus, the mechanism of enzymatic activation with a conformational change and/or the mechanism of binding to type-II kinase inhibitors may vary among protein kinases.

Sunintib is a clinically available multikinase inhibitor that is categorized as a type-I inhibitor. Interestingly, it displayed less inhibitory activity for phosphorylated VEGFR2 than for the non-phosphorylated enzyme. DiNitto et al. reported that Sunitinib binds to and stabilizes the inactive form of c-Kit, a tyrosine kinase from the same PDGFR superfamily as VEGFR2, and they concluded that Sunitinib only shows weak inhibition against activated c-Kit when its activation loop is phosphorylated.[30] In our study, a similar phenomenon might be in operation for phosphorylated VEGFR2, and Sunitinib might be a type-I inhibitor that preferentially targets the inactive forms of both c-Kit and VEGFR2.

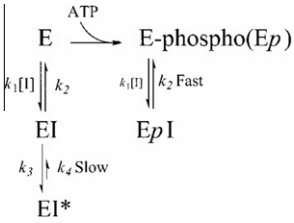

Scheme 3. Putative inhibitory mechanism of compound **20d** for non-phosphorylated and phosphorylated VEGFR2.

Recently, it was reported that the inhibitory activity of Axitinib, a type-II VEGFR2 kinase inhibitor, was strongly influenced by the juxtamembrane region of the enzyme and that Axitinib preferentially inhibited VEGFR2 protein with juxtamembrane domain rather than the catalytic domain.[31] Thus, there may be some structural regulation of VEGFR2 protein associated with the juxtamembrane domain. In the present study, however, we chose the catalytic domain of VEGFR2 because we wished to focus on binding events in the ATP-binding pocket to simplify analysis. In addition, it was considered difficult to obtain fully phosphorylated cytoplasmic domain enzyme through the autophosphorylation step with its weaker enzymatic activity than with the catalytic domain of the enzyme. Recently, we reported on the slow binding mechanism of TAK-593, another type-II VEGFR/PDGFR inhibitor and Sorafenib.[16] In that study, we performed activity and binding based analyses using the cytoplasmic domain of VEGFR2 with low phosphorylation, which contains the juxtamembrane domain, and we found that both TAK-593 and Sorafenib displayed two-step slow binding inhibition. Thus, the hypothesis for the behavior of type-II inhibitor suggested in this study may not only apply to the catalytic domain of VEGFR2 but also to the cytoplasmic domain of this enzyme.[16]

4. Conclusion

In conclusion, **20d** is an ATP competitive type-II VEGFR/PDGFR kinase inhibitor that is slow binding with and selective for non-phosphorylated VEGFR2. Its selective binding is driven by slow dissociation from non-phosphorylated VEGFR2. This study supports the theory that VEGFR2 kinase can adopt the DFG-out conformation (an inactive conformation) and bind with type-II inhibitors even after phosphorylation of tyrosine residues on its activation loop, but that binding of the inactive conformation with type-II inhibitors is not very stable, as was observed in the case of non-phosphorylated VEGFR2 (Scheme 3). Based on its slow dissociation, and supported by cellular wash-out experiments **20d** displays prolonged inhibitory activity in vitro and in vivo. These findings will help us to better understand the inhibitory mechanisms of type-I and type-II kinase inhibitors for non-phosphorylated and phosphorylated kinases and assist in the designing and synthesis of novel type-II kinase inhibitors. In particular, with these findings we demonstrate the importance of the dissociation rate determination from a kinase in distinct phosphorylation condition during the lead optimization of type-II kinase inhibitors.

5. Materials and methods

5.1. Chemicals

(1-{2-Fluoro-4-[(5-methyl-5*H*-pyrrolo[3,2-*d*]pyrimidin-4-yl)oxy]phenyl}-3-[3-(trifluoromethyl)phenyl]urea) (**20d**) was synthesized by Takeda Pharmaceutical Company, Ltd (Osaka, Japan).[15] Staurosporine was purchased from Wako Pure Chemicals (Osaka, Japan). Sorafenib (Nexavar®, Bayer, Germany) and Sunitinib (Sutent®, Pfizer, USA) were obtained from commercial sources.

5.2. Reagents

Ni-NTA resin was purchased from QIAGEN (Hilden, Germany). ATP, DTT, and puromycin were purchased from Sigma–Aldrich (MO, USA). AlphaScreen® Phosphotyrosine (P-Tyr 100) and AlphaScreen® Phosphotyrosine (PT66) assay kits were obtained from PerkinElmer (MA, USA). Biotinylated poly-GluTyr (4:1) was obtained from Cisbio (France). Anti-phospho-KDR/Flk-1/VEGFR2 (Tyr1054) and anti-phospho-KDR/Flk-1/VEGFR2 (Tyr1059) were obtained from Millipore (MA, USA). Block Ace® powder was purchased from Dainippon Sumitomo (Osaka, Japan) and sample treatment for Tris–SDS was purchased from Cosmobio (Tokyo, Japan). Phospho-tyrosine mouse mAb (P-Tyr-100), horseradish peroxidase-conjugated anti-rabbit IgG, 20× Lumi-GLO® Reagent and peroxide were obtained from Cell Signaling Technology (MA, USA), while VEGF Receptor 2 antibody for detection of total VEGFR2 was purchased from Abcam (Cambridge, UK). 5× Kinase Buffer A, Eu-anti-His-tag Antibody and Kinase Tracer 236 for the LanthaScreen™ Eu kinase binding assay were obtained from Invitrogen (CA, USA).

5.3. Cell culture and cellular autophosphorylation assay

Human embryonic kidney 293 cells stably expressing KDR (KDR/293) were purchased from Sibtech (CT, USA) and cultured in Dulbecco's modified Eagle's medium (DMEM; Invitrogen) supplemented with 10% fetal bovine serum (FBS; Moregate, Brisbane, Australia), 1× penicillin/streptomycin (Invitrogen), and 0.375 μg/ml of puromycin (Sigma–Aldrich) to maintain the expression of VEGFR2/KDR. Two days before the washout experiments, cells were seeded at 100,000/well in poly-D-lysine-coated 24-well plates. After 24 h, the medium was changed to DMEM containing 0.5% FBS, 1× penicillin/streptomycin, and 0.375 μg/ml of puromycin. Inhibitors prepared in DMSO were diluted with DMEM containing 0.5% FBS, 1× penicillin/streptomycin, and 0.375 μg/ml of puromycin, and then were added to the wells at 1 h before washout. After 1 h of exposure to each inhibitor, the wells were aspirated. Then the cells were washed three times with DMEM and stimulated with 50 ng/ml of VEGF (R&D Systems, MN, USA) at the indicated time after washout. Cellular autophsphorylation was detected by using a PathScan® Phospho-VEGFR-2 (Tyr1175) Sandwich ELISA Kit (Cell Signaling Technology) according to the manufacturer's instructions. Wells containing no test compound that were stimulated with VEGF and wells containing no compound without VEGF stimulation were used as the 100% control and 0% control, respectively.

5.4. VEGFR2 protein expression and auto-phosphorylation

The catalytic domain of human VEGFR2 (residues 806-1171) with deletion of the kinase insert domain (residues 940–989) was expressed as an N-terminal His-tagged protein with the TEV protease site by using a baculovirus expression system, as described previously.[15] Then 30 μM of purified VEGFR2 with its N-terminal His tag was subjected to auto-phosphorylation with 2 mM ATP and 10 mM $MgCl_2$ on ice for 90 min, after which the reaction mixture was desalted by using a HiPrep desalting column. Non-phosphorylated and phosphorylated VEGFR2 were stored at −80 °C.

5.5. Immunoblotting analysis

Protein samples were mixed with an equal volume of sample treatment for Tris–SDS (Cosmobio) containing 100 mM DTT and heated at 95 °C for 5 min. Then proteins were subjected to electrophoresis on SDS–polyacrylamide gel with Tris–glycine running

buffer, followed by electrotransfer to an iBlot PVDF Transfer Stack (Invitrogen) and incubation with 4% (w/v) Block Ace at 4 °C overnight. Then the membrane was washed and incubated at room temperature with anti-phospho or anti-VEGFR2 antibody (1:1000) for 1 h, after which it was incubated at room temperature with horseradish peroxidase-conjugated anti-rabbit IgG (1:1000) for 1 h and then visualized by using 1× LumiGLO® (Cell Signaling Technology) Reagent and peroxide.

5.6. Investigation of ATP-competitive inhibition of non-phosphorylated and phosphorylated VEGFR

VEGFR2 kinase activity was determined by using an anti-phosphotyrosine antibody with quantitation by the AlphaScreen® system[32] (PerkinElmer, USA). Enzyme reactions were performed in 50 mM Tris–HCl (pH 7.5), 5 mM $MnCl_2$, 5 mM $MgCl_2$, 0.01% Tween-20, and 2 mM DTT with ATP at various concentrations, 0.1 μg/ml biotinylated poly-GluTyr (4:1), and 75 pM of non-phosphorylated or phosphorylated VEGFR2. Reactions were initiated by adding VEGFR2 kinase to the reaction mixture and test compound, and reactions were quenched by the addition of 25 μl of 100 mM EDTA, 10 μg/ml each of AlphaScreen® streptavidin donor beads and acceptor beads in 62.5 mM HEPES (pH 7.4), 250 mM NaCl, and 0.1% BSA. Plates were incubated in the dark overnight and then read by an EnVision 2102 Multilabel Reader (PerkinElmer). Wells containing the substrate and the enzyme without **20d** were used as the total reaction control, while wells containing biotinylated poly-GluTyr (4:1) and the enzyme without ATP were used as the basal control. The concentration of **20d** producing 50% inhibition of the kinase activity of non-phosphorylated and phosphorylated VEGFR2 (IC_{50}) was analyzed using GraphPad Prism version 5.01 (GraphPad Software, CA, USA). Sigmoidal dose–response (variable slope) curves were fitted by non-linear regression analysis, with the top and bottom of the curve being constrained at 100 and 0, respectively.

5.7. Time-dependent inhibition of non-phosphorylated and phosphorylated VEGFR2

In order to assess the time-dependency of inhibition, assays were performed after pre-incubation of the enzyme with the inhibitor for various times and then conducting an enzyme activity assay where ATP was present at K_m^{app}. AlphaScreen® system, as described above was used to assay enzyme activity. By determining the IC_{50} value of **20d** as a function of enzyme–inhibitor pre-incubation time prior to initiation of catalysis we obtained a preliminary assessment of time dependent inhibition. IC_{50} values were calculated by logistic regression analysis (GraphPad Prism 5.01). Rigorous experiments to characterize the onset of inhibition consisted of the pre-incubation phase followed by dilution to 0.6 (15 μl initial to 25 μl final) upon addition of substrate. The enzyme activity phase of the experiments was conducted for 10 min. Eqs. 1a through 1d describe the fractional enzyme activity when accounting for the amount of additional onset of tight binding occurring during the activity phase of the assay. Fractional activity as a function of inhibitor concentration and pre-incubation time was fit globally to Eqs. 1a through 1d and overall quality of fit and consistency with other experimental data used to select the most appropriate binding model. Derivations of these equations are found in Supplementary data.

Single step with $k_{off} = 0$

$$\frac{E}{E_T} = e^{-k_{on}[I]t} e^{-k_{on}\frac{0.6[I]}{1+\frac{S}{K_M}}10} \tag{1a}$$

Full expression for single step

$$\frac{E}{E_T} = \frac{1}{1+\frac{0.6[I]}{\frac{k_{off}}{k_{on}}\left(1+\frac{S}{K_M}\right)}} + \frac{0.6[I]}{0.6[I]+\frac{k_{off}}{k_{on}}\left(1+\frac{S}{K_M}\right)} e^{-(k_{on}[I]+k_{off})t} e^{-\left(k_{on}\frac{0.6[I]}{1+\frac{S}{K_M}}+k_{off}\right)10} \tag{1b}$$

Two step with $k_{off} = 0$

$$\frac{E}{E_T} = \frac{e^{-k_3\frac{[I]}{[I]+K_I}t}}{1+\frac{0.6[I]}{K_I\left(1+\frac{S}{K_M}\right)}} e^{-k_3\frac{0.6[I]}{0.6[I]+K_I\left(1+\frac{S}{K_M}\right)}10} \tag{1c}$$

Full expression for two step

$$\frac{E}{E_T} = \frac{1}{1+\frac{0.6[I]}{K_I\left(1+\frac{S}{K_M}\right)}} \times \left[\frac{\beta}{\alpha+\beta} + \frac{\alpha}{\alpha+\beta} e^{-(\alpha'+\beta)t} e^{-(\alpha+\beta)10}\right] \tag{1d}$$

where:

$$\alpha = k_3 \frac{0.6[I]}{K_I\left(1+\frac{S}{K_M}\right)+0.6[I]}$$

$$\alpha' = k_3 \frac{[I]}{K_I+[I]}$$

$$\beta = k_4$$

Note: 0.6 corrects for inhibitor dilution and 10 min was the activity assay time.

With a two-step binding mechanism, the final equilibrium affinity of the inhibitor (K_i^*) is defined by Eq. 2.

$$K_i^* = k_4 K_i/(k_3+k_4) \tag{2}$$

The dissociation half-life ($t_{1/2}$) was calculated with Eq. 3

$$t_{1/2} = 0.693/k_4 \tag{3}$$

Eqs. 2 and 3 were previously described by Copeland.[33]

5.8. Determination of the dissociation rate constant by the rapid large dilution method

To determine the dissociation rate constant (k_{off}) of the inhibitors, enzyme–inhibitor dilution assays were performed. The assays involved determination of k_{off} from the kinetics of the recovery of kinase activity following rapid dilution of the enzyme–inhibitor complex.[33] Recovery of enzyme activity from a preformed enzyme–inhibitor complex was measured by using the AlphaScreen® system. The enzyme (at a 100-fold higher concentration than final activity conditions) and the inhibitor (at a 10-fold higher concentration than the initial IC_{50} value) were pre-incubated together in the reaction buffer for 60 min at room temperature permitting equilibrium formation for tight enzyme–inhibitor complexes. Then the complexes were diluted 1:100 in reaction buffer containing 1 mM ATP and 0.1 μg/ml biotinylated poly-Glu-Tyr (4:1) to initiate the kinase reaction. The kinetics of the recovery of kinase activity after rapid dilution were fitted to Eq. 4.[34]

Under the above conditions, k_{obs} represents k_{off} of the enzyme–inhibitor complex and the dissociation half-life ($t_{1/2}$) was calculated from Eq. 3 by replacement of k_4 with k_{obs}.

$$P = v_s t + [(v_i - v_s)/k_{obs}][1 - exp(-k_{obs})] + P0 \tag{4}$$

P; Product of the kinase reaction (CPS)
P0; Background signal when $t = 0$
v_i; Initial velocity
v_s; Steady state velocity
k_{obs}; Inhibition rate constant

5.9. Ligand displacement based dilution assay by use of LanthaScreen™ Eu kinase binding assay

Dissociation rate constants of inhibitors were determined by use of a ligand displacement based enzyme–inhibitor dilution assay. This assay involved determination of k_{off} through the kinetics of recovery of the tracer binding signal after rapid dilution of the enzyme–inhibitor complex. Recovery of the tracer binding signal from a preformed enzyme–inhibitor complex was measured by using the LanthaScreen™ Eu kinase binding assay. 500 nM of VEGFR2 enzyme (at a 100-fold higher concentration than the binding assay conditions) and the 1000 nM of inhibitor were incubated together in 1× Kinase Buffer A containing 2 mM DTT and 0.05% BSA for 60 min at ambient temperature to form the enzyme–inhibitor complex. Then the complex was diluted 1:100 in 1× Kinase Buffer A containing 2 mM DTT and 5 nM of Eu-anti-His-tag Antibody (Invitrogen) and 100 nM of Kinase Tracer 236 to initiate displacement of the inhibitor by an excess of Kinase Tracer 236. The kinetics of the recovery of tracer binding activity after rapid dilution were normalized as a percentage of tracer bound enzyme (100%; no inhibitor control, 0% no inhibitor and no enzyme control) and fitted to Eq. 5.

Under these conditions, k_{obs} represents k_{off} of the enzyme–inhibitor complex and the dissociation half-life was calculated with Eq. 3, replacing k_4 by k_{obs} in the same manner as for enzymatic activity based rapid dilution analysis.

$$Y = 100 - \mathrm{Span}(1 - \exp(-k_{obs}t)) \quad (5)$$

k_{obs}; rate constant for inhibition
Span; Y value when $t = \infty$

5.10. Binding kinetics analysis with a surface plasmon resonance (SPR) biosensor

To orthogonally determine the rate constants of association or dissociation, SPR experiments were performed with a Biacore 3000 biosensor (GE Healthcare, Fairfield, CT, USA) at 20 °C in 50 mM Tris–HCl (pH 7.5), 5 mM $MgCl_2$, 5 mM $MnCl_2$, 150 mM NaCl, 2 mM DTT, and 0.01% Surfactant P20 (GE Healthcare). Immobilization of non-phosphorylated VEGFR2 protein on the CM7 sensor chip (GE Healthcare) was conducted with the standard amine coupling procedure using 1 μM of protein and 10 μM of Staurosporine complex in 10 mM actetate (pH 6.0), 2 mM DTT, 5 mM $MgCl_2$, 5 mM $MnCl_2$, and 0.05% Surfactant P20. For phosphorylated VEGFR2 protein, immobilization was performed under the same conditions, except that the protein dilution buffer was 10 mM actetate (pH 5.0), 2 mM DTT, 5 mM $MgCl_2$, and 5 mM $MnCl_2$. Binding parameters were calculated globally from the obtained sensorgram data (RU) by fitting to a 1:1 interaction with the mass transfer model, except for Rmax values that were obtained by local fitting to the same binding model. SPR sensorgrams were analyzed with Biaevaluation software (GE Healthcare).

Acknowledgments

We thank Naoki Miyamoto, Yuya Oguro and Takaharu Hirayama for preparing compounds used in this study. We thank Shinji Tsuji and Yumi Hayano for preparation of recombinant human VEGFR2. We also thank Yumiko Moriya and Misae Abe for performing LC/MS analysis of the recombinant protein, as well as Taeko Yoshida for kind assistance with enzymatic assays and Ikuo Miyahisa for helpful discussion regarding analysis of the data from kinetic assays. Moreover, we thank Junji Matsui and Naoki Tarui for providing encouragement to undertake this study.

Supplementary data

Supplementary data (amino acid sequence of VEGFR2 is shown in Supplementary Figure S1. Results of LC/MS analysis of recombinant VEGFR2 proteins are shown in Supplementary Figure S2. Results of SPR analysis of Sorafenib binding with non-phosphorylated and phosphorylated VEGFR2 are shown in Supplementary Figure S3. Derivation of the equations describing onset of inhibition progress curve analysis is also shown) associated with this article can be found, in the online version, at doi:10.1016/j.bmc.2011.08.002.

References and notes

1. Manning, G.; Whyte, D. B.; Martinez, R.; Hunter, T.; Sudarsanam, S. *Science* **2002**, *298*, 1912.
2. Hubbard, S. R.; Till, J. H. *Ann. Rev. Biochem.* **2000**, *69*, 373.
3. Blume-Jensen, P.; Hunter, T. *Nature* **2001**, *411*, 355.
4. Hubbard, S. R.; Mohammadi, M.; Schlessinger, J. *J. Biol. Chem.* **1998**, *273*, 11987.
5. Traxler, P.; Furet, P. *Pharmacol. Ther.* **1999**, *82*, 195.
6. Schindler, T.; Bornmann, W.; Pellicena, P.; Miller, W. T.; Clarkson, B.; Kuriyan, J. *Science* **2000**, *289*, 1938.
7. Nagar, B.; Bornmann, W. G.; Pellicena, P.; Schindler, T.; Veach, D. R.; Miller, W. T.; Clarkson, B.; Kuriyan, J. *Cancer Res.* **2002**, *62*, 4236.
8. Kufareva, I.; Abagyan, R. *J. Med. Chem.* **2008**, *51*, 7921.
9. Pargellis, C.; Tong, L.; Churchill, L.; Cirillo, P. F.; Gilmore, T.; Graham, A. G.; Grob, P. M.; Hickey, E. R.; Moss, N.; Pav, S.; Regan, J. *Nat. Struct. Biol.* **2002**, *9*, 268.
10. Liu, Y.; Gray, N. S. *Nat. Chem. Biol.* **2006**, *2*, 358.
11. Angell, R. M.; Angell, T. D.; Bamborough, P.; Bamford, M. J.; Chung, C. W.; Cockerill, S. G.; Flack, S. S.; Jones, K. L.; Laine, D. I.; Longstaff, T.; Ludbrook, S.; Pearson, R.; Smith, K. J.; Smee, P. A.; Somers, D. O.; Walker, A. L. *Bioorg. Med. Chem. Lett.* **2008**, *18*, 4433.
12. Morphy, R. *J. Med. Chem.* **2010**, *53*, 1413.
13. Bull, H. G.; Thornberry, N. A.; Cordes, M. H.; Patchett, A. A.; Cordes, E. H. *J. Biol. Chem.* **1985**, *260*, 2952.
14. Garvey, E. P.; Schwartz, B.; Gartland, M. J.; Lang, S.; Halsey, W.; Sathe, G.; Carter, H. L., 3rd; Weaver, K. L. *Biochemistry* **2009**, *48*, 1644.
15. Oguro, Y.; Miyamoto, N.; Okada, K.; Takagi, T.; Iwata, H.; Awazu, Y.; Miki, H.; Hori, A.; Kamiyama, K.; Imamura, S. *Bioorg. Med. Chem.* **2010**, *18*, 7260.
16. Iwata, H.; Imamura, S.; Hori, A.; Hixon, M. S.; Kimura, H.; Miki, H. *Biochemistry* **2011**, *50*, 738.
17. Dougher, M.; Terman, B. I. *Oncogene* **1999**, *18*, 1619.
18. Shah, P. P.; Myers, M. C.; Beavers, M. P.; Purvis, J. E.; Jing, H.; Grieser, H. J.; Sharlow, E. R.; Napper, A. D.; Huryn, D. M.; Cooperman, B. S.; Smith, A. B., 3rd; Diamond, S. L. *Mol. Pharmacol.* **2008**, *74*, 34.
19. Han, S.; Mistry, A.; Chang, J. S.; Cunningham, D.; Griffor, M.; Bonnette, P. C.; Wang, H.; Chrunyk, B. A.; Aspnes, G. E.; Walker, D. P.; Brosius, A. D.; Buckbinder, L. *J. Biol. Chem.* **2009**, *284*, 13193.
20. Takahashi, T.; Yamaguchi, S.; Chida, K.; Shibuya, M. *EMBO J.* **2001**, *20*, 2768.
21. Dougher-Vermazen, M.; Hulmes, J. D.; Bohlen, P.; Terman, B. I. *Biochem. Biophys. Res. Commun.* **1994**, *205*, 728.
22. Meyer, R. D.; Latz, C.; Rahimi, N. *J. Biol. Chem.* **2003**, *278*, 16347.
23. Zhao, G.; Peery, R. B.; Yingling, J. M. *Anal. Biochem.* **2007**, *360*, 196.
24. Miyazaki, Y.; Matsunaga, S.; Tang, J.; Maeda, Y.; Nakano, M.; Philippe, R. J.; Shibahara, M.; Liu, W.; Sato, H.; Wang, L.; Nolte, R. T. *Bioorg. Med. Chem. Lett.* **2005**, *15*, 2203.
25. Yang, J.; Zappacosta, F.; Annan, R. S.; Nurse, K.; Tummino, P. J.; Copeland, R. A.; Lai, Z. *Biochem. J.* **2009**, *417*, 355.
26. Sullivan, J. E.; Holdgate, G. A.; Campbell, D.; Timms, D.; Gerhardt, S.; Breed, J.; Breeze, A. L.; Bermingham, A.; Pauptit, R. A.; Norman, R. A.; Embrey, K. J.; Read, J.; VanScyoc, W. S.; Ward, W. H. *Biochemistry* **2005**, *44*, 16475.
27. Vogtherr, M.; Saxena, K.; Hoelder, S.; Grimme, S.; Betz, M.; Schieborr, U.; Pescatore, B.; Robin, M.; Delarbre, L.; Langer, T.; Wendt, K. U.; Schwalbe, H. *Angew. Chem., Int. Ed.* **2006**, *45*, 993.
28. Frembgen-Kesner, T.; Elcock, A. H. *J. Mol. Biol.* **2006**, *359*, 202.
29. Filomia, F.; De Rienzo, F.; Menziani, M. C. *Bioorg. Med. Chem.* **2010**, *18*, 6805.
30. DiNitto, J. P.; Deshmukh, G. D.; Zhang, Y.; Jacques, S. L.; Coli, R.; Worrall, J. W.; Diehl, W.; English, J. M.; Wu, J. C. *J Biochem* **2010**, *147*, 601.
31. Solowiej, J.; Bergqvist, S.; McTigue, M. A.; Marrone, T.; Quenzer, T.; Cobbs, M.; Ryan, K.; Kania, R. S.; Diehl, W.; Murray, B. W. *Biochemistry* **2009**, *48*, 7019.
32. Ullman, E. F.; Kirakossian, H.; Singh, S.; Wu, Z. P.; Irvin, B. R.; Pease, J. S.; Switchenko, A. C.; Irvine, J. D.; Dafforn, A.; Skold, C. N. *Proc. Natl. Acad. Sci. U.S.A.* **1994**, *91*, 5426.
33. Copeland, R. A. *Methods Biochem. Anal.* **2005**, *46*, 1.
34. Morrison, J. F.; Walsh, C. T. *Adv. Enzymol. Relat. Areas Mol. Biol.* **1988**, *61*, 201.